Investigation on high-κ dielectric for low leakage AlGaN/GaN MIS−HEMT device, using material selection methodologies

© *Baikadi Pranay Kumar Reddy, Karri Babu Ravi Teja, Kavindra Kandpal*¶

Department of Electrical & Electronics Engineering,
Birla Institute of Technology and Science Pilani,
Rajasthan, India

¶ E-mail: kavindra.kandpal@pilani.bits-pilani.ac.in, f2014465@pilani.bits-pilani.ac.in, baburaviteja.k@pilani.bits-pilani.ac.in

(Received 15.05.2017. Received ofter revision 11.12.2017)

This paper analyzes various high-κ dielectrics for low leakage AlGaN (Aluminium Gallium Nitride)/GaN (Gallium Nitride) MIS-HEMT (Metal Insulator Semiconductor — High Electron Mobility Transistor) device. The investigation is carried out by examining different attributes such as the dielectric constant, conduction band offset, and energy band gap of the dielectric which are crucial for a good dielectric-AlGaN interface. This work also computes the values of band offsets of different dielectrics to AlGaN analytically. The selection of the most promising dielectric is done using three different multi-criteria decision making methods (MCDM) namely the Ashby, VIKOR (VIseKriterijumska Optimizacija I Kompromisno Resenje in Serbian, meaning Multicriteria Optimization and Compromise Solution) and TOPSIS (Technique for Order Preference by Similarity to Ideal Solution). All the analyses point to La_2O_3 as the best gate dielectric for AlGaN/GaN MIS−HEMT device.

1. Introduction

Ever since the advent of silicon based transistor by Morris Tanenbaum in 1954 [1], these silicon based transistors have been the figurehead of the semiconductor industry. An innumerable number of ingenious products were made possible with these silicon based transistors serving as the building blocks. The size of the transistors also decreased dramatically with gate lengths ranging from around 10 μm in the early 1970s to as low as 10 nm FinFET reported in recent years [2]. The silicon based transistors have thus reached a point where major performance improvements are difficult to achieve. Moreover, with the genesis of various power electronic applications, the demand for transistors with high breakdown voltage, high switching speeds and low leakage currents has risen. This led to the search for other possible semiconductor materials.

The AlGaN/GaN heterostructure is considered as a potential alternative to replace the conventional silicon based device because of high breakdown field, wide band gap and large carrier concentration. The device structure of the MIS−HEMT is depicted in the Fig. 1. GaN here acts as the narrow band gap semiconductor ($E_g = 3.2$ eV) and AlGaN acts as the wide band gap semiconductor ($E_g = 3.89$ eV). Once the semiconductors come in contact with each other, a triangular potential well is formed because of the discontinuity in conduction band between the two semiconductors. As a result, the electrons get trapped in this quantum well which leads to the formation of a 2DEG (Two-Dimensional Electron Gas) near the boundary at the bottom of $Al_{0.3}Ga_{0.7}N$. The mechanism of formation of the 2DEG in AlGaN−GaN is well established [3] and is attributed to the spontaneous and piezoelectric polarizations of AlGaN. This 2DEG makes the HEMT devices as excellent candidates for high frequency and high power applications. A simple Schottky gate HEMT, however, suffers from high gate leakage current [4] which could lead to unwanted power losses which ultimately leads to degradation of output power efficiency. The best alternative to reduce the high leakage current of Schottky gate HEMTs is to deposit a layer of dielectric on AlGaN. A number of high-κ dielectrics, including La_2O_3, Si_3N_4, ZrO_2, TiO_2, Y_2O_3 [5–9] have been reported in the literature where the deposition of the dielectric reduces gate leakage current by several orders of magnitude. However, each dielectric has its own advantages and also practical limitations. Furthermore, the

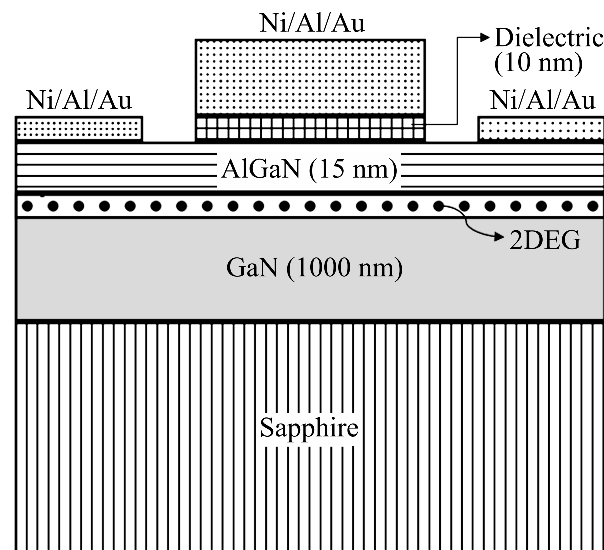

Figure 1. Structure of AlGaN/GaN MIS−HEMT device.

different properties of the dielectric which minimize the leakage current are themselves not exclusive. A number of tradeoffs exist between these properties of the dielectric and hence the selection of optimum dielectric directly is not possible. For example, the dielectric constant and energy band gap of the dielectric are inversely related. Such tradeoffs make it difficult to select the optimum dielectric material for the device. These cases however, are well handled with the use of Multiple Criteria Decision Making (MCDM) methods as reported in many scientific and industrial regimes [10–12].

In this paper, different dielectrics are investigated to determine the best alternative for AlGaN−GaN HEMT device. Specifically, $Al_{0.3}Ga_{0.7}N$ is used here although other alloys of AlGaN can also be used for the analysis. The key parameters that are necessary for dielectric selection are dielectric constant, band alignment with $Al_{0.3}Ga_{0.7}N$, magnitude of thermal mismatch with $Al_{0.3}Ga_{0.7}N$ and the energy band gap (E_g) of the dielectric. All these attributes of the dielectrics are used as an input to the standard MCDM methods namely the Ashby, VIKOR and TOPSIS and these methods are applied to select the best dielectric.

The organization of the paper is as follows: Section 2 deals with the various performance criteria used for evaluating the performance of a dielectric. Section 3 discusses different material selection methodologies that are used in this present work where each methodology is explained in detail. This is followed by the results of ASHBY, TOPSIS and VIKOR methods in Section 4 and finally, Section 5 provides the conclusions drawn from the study.

2. Performance attributes of different Dielectrics

For any MIS−HEMT device, gate leakage current and breakdown voltage serve as the measure of reliability of the device. Hence, those parameters of the dielectric which affect the gate leakage current and breakdown voltage have to be carefully selected for evaluating the performance of the dielectric when it is incorporated in the device. For a given dielectric material, energy band gap (E_g), conduction band offset (CBO) to the underlying material ($Al_{0.3}Ga_{0.7}N$ in this case), dielectric constant (κ) and the magnitude of thermal mismatch —ΔTEC— are the crucial parameters which affect the leakage current

and the breakdown voltage. E_g and breakdown electric field for a dielectric are directly related by

$$E_{BII} = 1.36 \cdot 10^7 \frac{E_g}{4.0} \text{ V/cm}, \tag{1}$$

where E_{BII} refers to the breakdown electric field of the dielectric [13]. Therefore, to have a higher breakdown electric field one needs a dielectric with higher E_g.

Another important performance parameter while selecting the dielectric is the dielectric constant κ. The importance of κ (represented here by C_{ox}) can be explained using the Eq. (2) where C_{ox} is the capacitance per unit area of the dielectric

$$C_{ox} = \frac{\varepsilon_{ox}\varepsilon_o A}{t_{ox}}. \tag{2}$$

For the MIS−HEMT device, higher value of C_{ox} leads to a higher value of drain to source current for a given value of applied gate to substrate voltage. From the Eq. (2), it is evident that C_{ox} can be increased either by reducing the dielectric thickness t_{ox} or by increasing the dielectric constant κ_{ox}. However, reducing the thickness of dielectric has the adverse effects of increased gate tunnelling current which is not desirable. Hence, using a high-κ dielectric will increase the dielectric capacitance thereby increasing the drain to source current in the device. Another advantage of using high-κ material is that, for a given C_{ox} a thicker dielectric can be used which in turn decreases the gate leakage current.

The gate leakage current in any MIS−HEMT device is dominated by the Poole−Frenkel conduction mechanism [14–16] and is given by

$$J \propto E \exp\left(\frac{-q\varphi_b - \sqrt{\frac{qE}{\pi\varepsilon_j}}}{kT}\right), \tag{3}$$

where q is the charge of electron, φ_b is the CBO of the dielectric to AlGaN, E is the electric field inside the dielectric, ε_i is the dielectric constant, k is the Boltzmann constant and T is the absolute temperature. It is evident from Eq. (3) that a higher value of CBO provides a greater barrier for the electrons and thus limits the leakage current. The conventional Schottky gate HEMT suffers from high gate leakage current, so a dielectric which provides a greater CBO is naturally preferred as it reduces the gate leakage current.

The deposition of the dielectric on AlGaN generally takes place at elevated temperatures or subjected to thermal annealing. Thermal mismatch between AlGaN and dielectric layer therefore, becomes another crucial parameter as it can result in either compressive or tensile stress at the semiconductor-dielectric interface. A higher value of mismatch leads to greater interfacial defects which would increase the leakage current. The dielectric constant and band gap values of the dielectrics are readily available in the literature [17]. Conduction band offset values on AlGaN, however, are not available in the literature. Anderson's rule [18] gives CBO as the difference in electron affinities of the two materials

$$\Delta E_c = X_2 - X_1. \tag{4}$$

However, this rule was shown to give highly inconsistent [19] when applied to heterostructures as it assumes the absence of both interface states and surface states which clearly are present in many heterostructures, including the AlGaN/GaN and hence is avoided in the current work. Instead these values are computed using the Charge Neutrality Level (CNL) method.

CNL is level of Fermi Level which renders the surface without a net charge. CNL method showed extremely promising results when band offsets were calculated between various oxides and silicon [20]. In the current work, band offsets are to be calculated to $Al_{0.3}Ga_{0.7}N$ instead of silicon. The equation

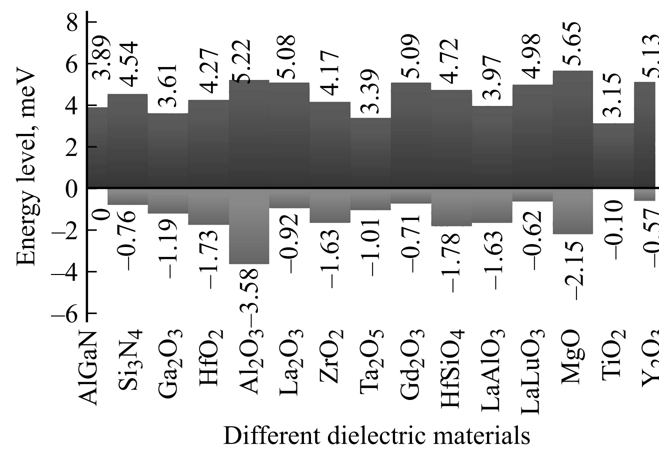

Figure 2. VBO and CBO of different dielectrics to $Al_{0.3}Ga_{0.7}N$.

describing the relation between CBO and CNL levels is well documented in the work of Robertson and Falabretti [21] which is restated in the Eq. (5).

$$\phi_n = (X_a - \phi_{sa}) - (X_b - \phi_{sb}) + S(\phi_{sa} - \phi_{sb}), \tag{5}$$

where the CNL values ϕ_{sa}, ϕ_{sb} are measured from the vacuum level, S is the Schottky Pinning Factor of the wide band-gap semiconductor (dielectric in this case) and X_a, X_b are the electron affinities of semiconductors a and b, respectively. The CNL values used in the current work are measured from top of the valence band. This is done by modifying Eq. (5) as,

$$\begin{aligned}\phi_n &= (X_a - \phi_{sa}) - (X_b - \phi_{sb}) + S(\phi_{sa} - \phi_{sb})\\ &= \big(X_a - (E_{ga} + X_a - \phi'_{sa})\big) - \big(X_b - (E_{gb} + X_b - \phi'_{sb})\big)\\ &+ S\big((E_{ga} + X_a - \phi'_{sa}) - (E_{gb} + X_b - \phi'_{sb})\big) = (X_a - X_b)\\ &+ (S-1)\big(X_a - X_b + E_{ga} - E_{gb} - (\phi'_{sa} - \phi'_{sb})\big),\end{aligned} \tag{6}$$

where ϕ'_{sa}, ϕ'_{sb} are the CNL levels of semiconductors a and b measured from top of the valence band. For the current work, „a“ in the Eq. (6) is $Al_{0.3}Ga_{0.7}N$ and „b“ is the dielectric material.

The CNL value of $Al_xGa_{1-x}N$ [22] is given by

$$\mathrm{CNL}(\mathrm{Al}_x\mathrm{Ga}_{1-x}\mathrm{N}) = xX(\mathrm{AlN}) + (1-x)X(\mathrm{GaN}), \tag{7}$$

where X (AlN)is the electron affinity of Aluminium Nitride and X (GaN) is the electron affinity of Gallium Nitride. For the current work, x is 0.3 which gives a value of 2.3 eV as the electron affinity of $Al_{0.3}Ga_{0.7}N$, which is acceptable as the electron affinity of AlN is 0.6 eV [21] and that of GaN is 3.3 eV [21]. The Energy band gap of $Al_{0.3}Ga_{0.7}N$ is given by the Eq. (8), where the value of x is 0.3 in this case [23]

$$E_g(\mathrm{Al}_x\mathrm{Ga}_{1-x}\mathrm{N}) = xE_g(\mathrm{AlN}) + (1-x)E_g(\mathrm{GaN}) - bx(1-x). \tag{8}$$

The constant b is known as the bowing parameter and values of b varying from 0.53 to 2.6 eV [24] have been reported in the literature. In the present work, the value of b is taken as 1 eV [25]. This gives a value of 3.89 eV as the band gap of $Al_{0.3}Ga_{0.7}N$. This is a reasonable value as this value falls in between E_g of AlN (6.2 eV) [17] and E_g of GaN (3.2 eV) [17] as is expected. The value of electron affinity for $Al_{0.3}Ga_{0.7}N$ reported in the literature is 2.3 eV [23] which is sufficiently validated by the fact that this

Table 1. Calculated results of CBO of all dielectrics through CNL method

Dielectric	X, eV	CNL, eV	S	CBO
Si_3N_4	2.1	2.6	0.59	0.651
Ga_2O_3	3.5	2.8	0.49	−0.282
HfO_2	2.4	3.7	0.52	0.38
Al_2O_3	1	6	0.69	1.331
La_2O_3	2	2.4	0.53	1.193
ZrO_2	2.5	3.6	0.52	0.28
Ta_2O_5	3.3	3.3	0.4	−0.58
Gd_2O_3	2.4	2.3	0.41	1.198
$HfSiO_4$	2	3.6	0.56	0.828
$LaAlO_3$	2.5	3.8	0.53	0.082
$LaLuO_3$	1.3	3	0.53	1.094
MgO	0.8	4	0.71	1.761
TiO_2	3.9	2.2	0.18	−0.739
Y_2O_3	1.84	2.4	0.46	1.2376

Table 2. Performance matrix of different dielectrics

Dielectric	Dielectric constant, κ	E_g, eV	CBO, eV	$\lvert\Delta TEC\rvert$
Si_3N_4	7	5.3	0.651	12.2
Ga_2O_3	23	4.8	−0.282	7.7
HfO_2	25	6	0.38	1.04
Al_2O_3	9	8.8	1.331	6.6
La_2O_3	30	6	1.193	6.4
ZrO_2	25	5.8	0.28	7.7
Ta_2O_5	22	4.4	−0.58	10
Gd_2O_3	16	5.8	1.198	11.76
$HfSiO_4$	11	6.5	0.828	16.8
$LaAlO_3$	30	5.6	0.082	3.4
$LaLuO_3$	32	5.6	1.094	8.7
MgO	9.8	7.8	1.761	4.2
TiO_2	80	3.05	−0.739	4.9
Y_2O_3	15	5.7	1.2376	7.6

value falls in between the electron affinities of AlN (0.6 eV) [17] and GaN (3.3 eV) [17]. The calculated values of CBO are presented in Table 1. The Valence Band Offset (VBO) and Conduction Band Offset (CBO) of various dielectrics are pictorially represented in Fig. 2.

The final performance criterion is thermal mismatch between the dielectric and $Al_{0.3}Ga_{0.7}N$. The thermal expansion coefficient (TEC) values of different dielectric material available in the literature [26–29]. The value of TEC for AlGaN as reported in the literature is 15 ppm per Kelvin [30] and the mismatches are calculated by taking the magnitude of difference in TEC values of dielectric and $Al_{0.3}Ga_{0.7}N$ irrespective of the nature of stress, i. e. whether the stress is tensile or compressive. The complete performance matrix consisting of CBO, E_g, κ, $|\Delta TEC|$ is depicted in Table 2.

3. Material selection methodologies

MCDM methodologies serve as an exceptional tool when a decision has to be made in regard to choose a material out of a pool of materials which are characterized by various attributes. These methodologies are extensively studied and are widely used in scientific and engineering regimes [10–12]. Out of the various MCDM approaches, the three most popular approaches are the Ashby's approach, the VIKOR approach, and the TOPSIS approach.

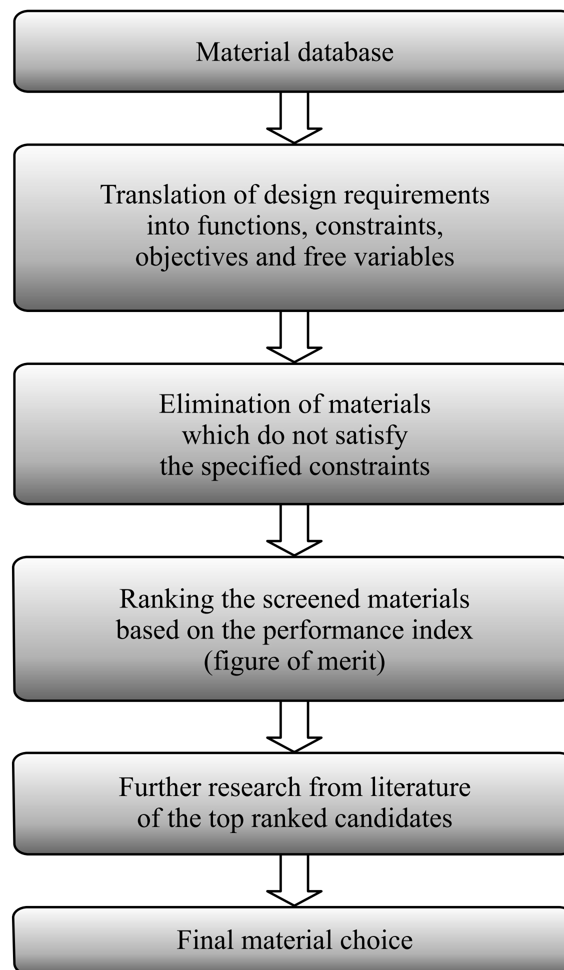

Figure 3. Flow chart of the Ashby's approach.

3.1. Ashby's Method

Ashby analysis, proposed by Michael Ashby [31,32], is a free-search selection methodology which has the advantage of being intuitive and relatively simple with a limited number of calculations. The flow of the Ashby analysis is described in the Fig. 3. The analysis starts with the translation step where the design requirements are converted into objectives and constraints which can then be used to identify the materials. The next step is the screening of materials which does not satisfy the design constraints. This is done by sketching scatter plots between various material indices taken two at a time and finding out the set of materials that satisfy the design requirements. The final set of materials which satisfy all the constraints is obtained by taking the intersection of the all the sets of materials from each of the scatter plot. Following this step, the screened materials are ranked based on a performance index which explicitly quantifies how desirable a particular material is in a specific situation. The final material choice is made by doing further research on the top ranked materials.

The objective is to minimize the gate leakage currents and also increase the breakdown electric field. The following constraints are used for the Ashby analysis:

a) dielectric constant (κ) greater than 15 eV [33];
b) conduction Band Offset (CBO) greater than 1 eV [33];
c) band gap (E_g) of dielectric greater than 5 eV [34].

As mentioned in Section 2, the gate leakage current is dominated by the Poole–Frenkel conduction mechanism. The leakage current density given in Section 2 is restated here as Eq. (9)

$$J \propto E \exp\left(\frac{-q\left(\varphi_b - \sqrt{\frac{qE}{\pi\varepsilon_i}}\right)}{kT}\right). \tag{9}$$

Once the Ashby analysis is done with the constraints mentioned above, a set of dielectrics which satisfy all the three mentioned above will be obtained. In order to choose the best dielectric among the set of dielectrics obtained, one has to define a figure of merit which quantitatively justifies which of those dielectrics minimizes the objective function, which is the gate leakage current in this case. To achieve this, the Eq. (9) is reframed as

$$J = aE \exp(-f), \tag{10}$$

where

$$f = \frac{q\left(\varphi_b - \sqrt{\frac{qE}{\pi\varepsilon_i}}\right)}{kT}$$

and a is a constant.

From the Eq. (10) it can be deduced that dielectrics with positive values of f are preferred as they offer smaller leakage current and negative values of f indicates greater leakage current.

3.2. TOPSIS approach

TOPSIS approach was proposed by Hwang and Yoon in 1981 [35]. TOPSIS is attractive because only a limited subjective input is needed from the decision makers. This approach is based on the factor that the best alternative should have the shortest Euclidean distance (S^*) from the ideal solution (A^*) and the largest Euclidean distance (S^-) from the non-ideal solution (A^-). The flow chart for the TOPSIS approach is given in the Fig. 4.

The five main steps that are involved in the TOPSIS approach [35] are:

Step 1: TOPSIS approach starts by normalizing each material index for every element. The normalized decision matrix value for i^{th} element under j^{th} criterion is given by:

$$N_{ij} = \frac{x_{ij}}{\sqrt{\Sigma_{i=1}^{p} x_{ij}}}, \tag{11}$$

where i$= 1, 2, 3, \ldots, p$, represents the different materials and $j = 1, 2, 3, \ldots, q$, represents different material indices.

Step 2: Once the Normalized matrix is obtained, the Weighted Normal Matrix (M_{ij}) is got by choosing weights w_j appropriately such that each weight justifies the importance of the corresponding attribute in optimizing the design requirement and parallely satisfying the equation $\sum_{j=1}^{q} w_j = 1$. An element M_{ij} of the Weighted Normal Matrix is given by $M_{ij} = N_{ij} w_j$.

Step 3: The ideal solution is identified as $A^* = \max(M_{ij}, j \in J_1)$ or $\min(M_{ij}, j \in J_2)$, where J_1 is the set of all indices which denote the benefit criteria and J_2 is the set of all indices which denote the cost criteria.

The non ideal solution is identified as $A^- = \min(M_{ij}, j \in J_1)$ or $\max(M_{ij}, j \in J_2)$, where J_1 is the set of all indices which denote the benefit criteria and J_2 is the set of all indices which denote the cost criteria.

Step 4: Now that ideal and non ideal solutions are identified, one has to compute the Euclidean distance of each material from the ideal and non ideal solutions. The distance from the ideal solution is

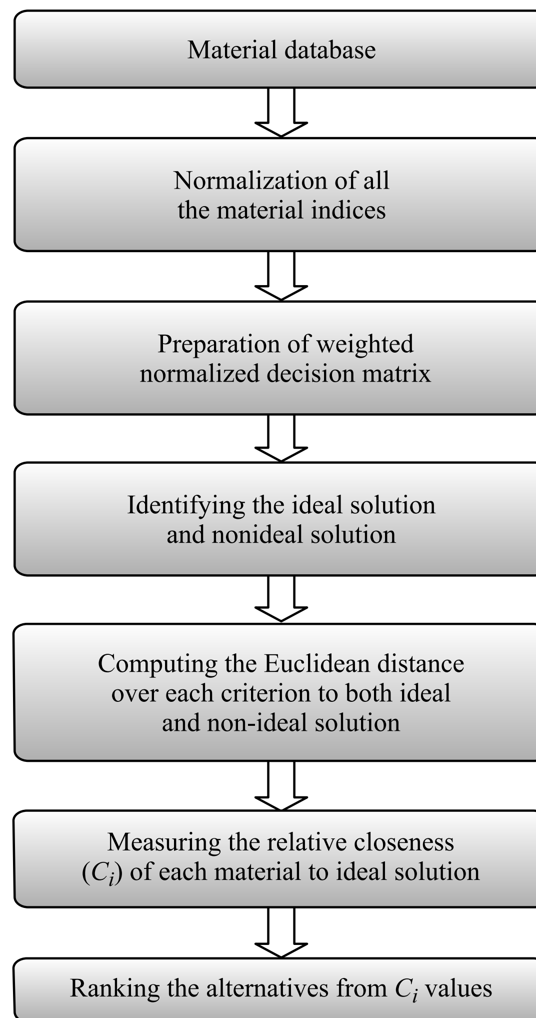

Figure 4. Flow chart for TOPSIS approach.

given by:

$$S_i^* = \sqrt{\sum_{j=1}^{q} (M_{ij} - M_j^*)^2}, \tag{12}$$

where M_j^* denotes the ideal value of the jth index.

The distance from the non-ideal solution is given by:

$$S_i^- = \sqrt{\sum_{j=1}^{q} (M_{ij} - M_j^-)^2}, \tag{13}$$

where, M_j^- denotes the non-ideal value of the jth index. Both the distances are computed for $i = 1, 2, 3, \ldots, p$.

Step 5: The relative closeness (C_i) is computed as:

$$C_i = \frac{S_i^-}{S_i^- + S_i^*} \quad 0 < C_i < 1 \text{ for } i = 1, 2, 3, \ldots, p.$$

Hence, a larger value of C_i implies that the alternative is farther from the non-ideal solution. Correspondingly the ranking of the alternatives is done based on the value of C_i, with greater value of C_i implying that the material gives a better performance.

3.3. VIKOR approach

VIKOR approach works by ranking and selecting from alternatives based on the indices and follows the approach of closeness-to-ideal. It was first proposed by Serafim Opricovic in 1998 [36] and it serves as an efficient tool to handle conflicting criteria. A modified version was later proposed by Chang [37] which greatly simplified the numerical calculations in solving the problems. In this method, the alternatives are ranked and a compromise solution is determined that is closest to the ideal solution. The flow chart for VIKOR analysis is shown in the Fig. 5.

The five main steps that are involved in the VIKOR approach are:

Step 1: Determine the best value x_j^* and the worst value x_j^- for each of the material indices based on the following equations:
$x_j^* = \max(x_{ij})$ and $x_j^- = \min(x_{ij})$ if j^{th} criterion is a benefit criterion and $x_j^* = \min(x_{ij})$ and $x_j^- = \max(x_{ij})$ if j^{th} criterion is a cost criterion for $i = 1, 2, 3, \ldots, p$.

Step 2: The maximum utility group (G_i) is constructed as:

$$G_i = \sum_{j=1}^{q} w_j \frac{x_j^* - x_{ij}}{x_j^* - x_j^-}, \tag{14}$$

where, w_j's are appropriately chosen such that each weight signifies the importance of that particular attribute in optimizing the design requirement and also $\sum_{j=1}^{q} w_j = 1$. Similarly maximum regret group is

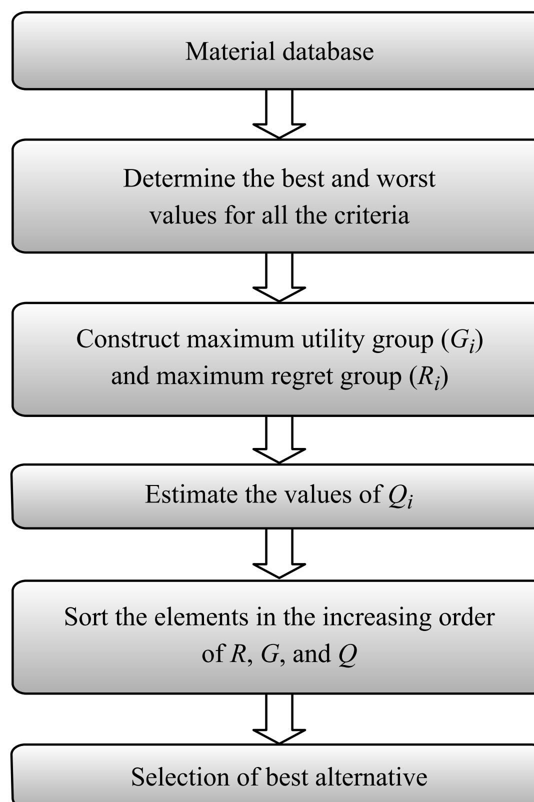

Figure 5. Flow chart of VIKOR approach.

formulated as:

$$R_i = \max_j \left(w_j \frac{x_j^* - x_{ij}}{x_j^* - x_j^-} \right). \tag{15}$$

Step 3: Q_i value for the ith alternative for $i = 1, 2, 3, \ldots, p$ is calculated as given by:

$$Q_i = \sigma \frac{G_i - G^*}{G^- - G^*} + (1 - \sigma) \frac{R_i - R^*}{R^- - R^*}, \tag{16}$$

where, $G^* = \min G_i$ and $G^- = \max G_i$, $R^* = \max R_i$ and $R^- = \min R_i$. The value of σ is usually taken to be 0.5.

Step 4: All the alternatives are arranged in the increasing order of R, G and Q values and hence the order ranking $(A^1, A^2, A^3, \ldots, A^p)$ is computed.

Step 5: Once the alternatives are arranged in increasing order of R, G and Q values, $Q(A^2) - Q(A^1)$ is computed and is compared with DQ, where $DQ = 1/(N-1)$. If the value is greater than DQ and if the A^1 is best ranked in R and G as well, then A^1 is declared as the best dielectric. If the condition is not satisfied, then all the alternatives which satisfy $Q(A^u) - Q(A^1) \leq DQ$ are declared as the best alternatives.

4. Results and Discussions

4.1. Ashby analysis

The preliminary step in Ashby approach is to plot the graphs between various material indices. Later the constraints mentioned in section 3.1 are applied to find out the best set of dielectrics.

The plot between CBO and κ of various dielectrics is shown in the Fig. 6. For a given dielectric to perform efficiently one needs a band offset greater than 1 eV and dielectric constant greater than 15. The dielectrics which satisfy these criteria are enclosed in the rectangle in the Fig. 6, which are Y_2O_3, Gd_2O_3, $LaLuO_3$ and La_2O_3.

Fig. 7 shows the plot between E_g and κ of all the mentioned dielectrics. One needs a band gap greater than 5 eV and as mentioned before, a dielectric constant greater than 15. These criteria are satisfied by Y_2O_3, Gd_2O_3, $LaLuO_3$, La_2O_3, HfO_2 and ZrO_2 as by the rectangle enclosing them in Fig. 7.

Finally, the plot between CBO and E_g is shown in the Fig. 8. As mentioned earlier, one needs a CBO greater than 1 eV and E_g greater than 5 eV. These two criteria are satisfied by Y_2O_3, Gd_2O_3, $LaLuO_3$, La_2O_3, MgO, SiO_2 and Al_2O_3 as shown by the rectangle enclosing them in Fig. 8.

So, clearly, Y_2O_3, Gd_2O_3, $LaLuO_3$, La_2O_3 are the only dielectrics which satisfy all the three decision criteria. The best dielectric among these is selected based on the figure of merit (f), which is shown

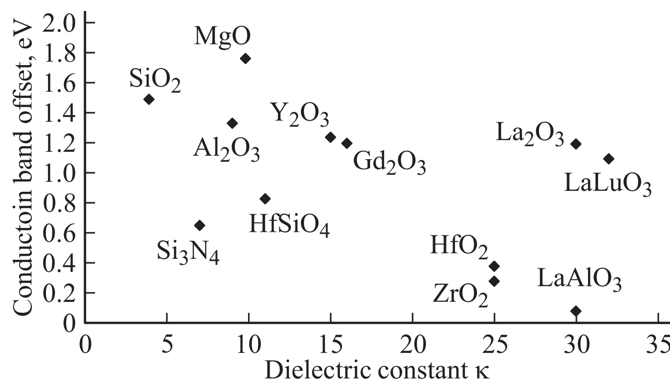

Figure 6. CBO vs. Dielectric Constant.

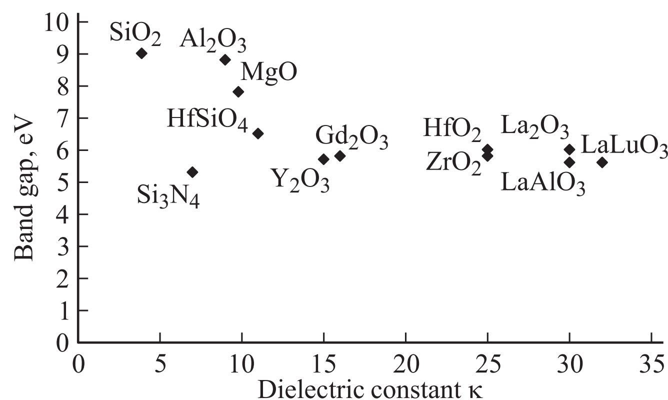

Figure 7. Band Gap vs. Dielectric Constant.

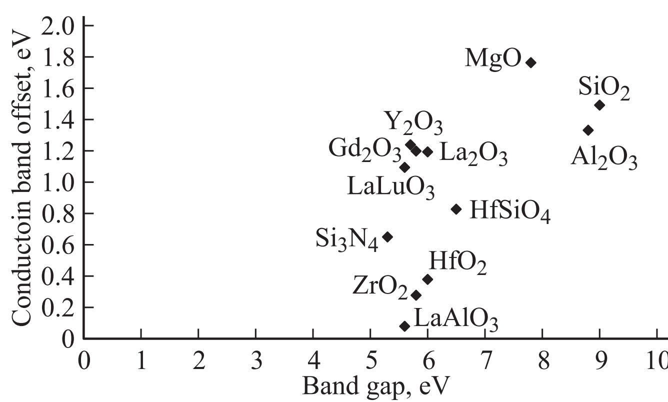

Figure 8. Conduction Band Offset vs. Band Gap.

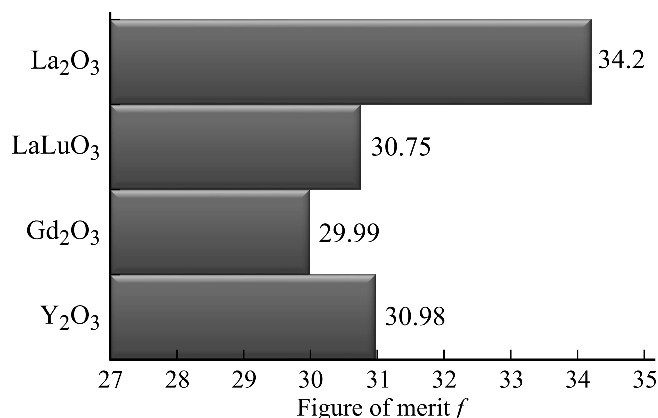

Figure 9. Plot of figure of merit of different dielectrics.

in Fig. 9. One can clearly see from the plot that La_2O_3 has the best figure of merit among the four dielectrics mentioned above. Hence it can be concluded that Ashby analysis gives La_2O_3 as the best dielectric among the stated dielectrics.

4.2. TOPSIS analysis

To perform the TOPSIS analysis one needs a weighted normal matrix. The weighted normal matrix for the current work is given in Table 3. From the Poole–Frenkel conduction equation stated in

Table 3. Weighted Normal Matrix

Dielectric	0.3*, [K]	0.4* [CBO]	0.2* [E_g]	0.1* [ΔCTE]
Si_3N_4	0.018923	0.072896	0.047652	0.037468
Ga_2O_3	0.062177	−0.03158	0.043157	0.023648
HfO_2	0.067584	0.042551	0.053946	0.003194
Al_2O_3	0.02433	0.14904	0.079121	0.02027
La_2O_3	0.081101	0.133587	0.053946	0.019655
ZrO_2	0.067584	0.031353	0.052148	0.023648
Ta_2O_5	0.059474	−0.06495	0.039561	0.030712
Gd_2O_3	0.043254	0.134147	0.052148	0.036117
$HfSiO_4$	0.029737	0.092716	0.058442	0.051595
$LaAlO_3$	0.081101	0.009182	0.05035	0.010442
$LaLuO_3$	0.086507	0.122502	0.05035	0.026719
MgO	0.026493	0.19719	0.07013	0.012899
TiO_2	0.216269	−0.08275	0.027423	0.015049
Y_2O_3	0.04055	0.138581	0.051249	0.023341

Table 4. Results and Ranking of TOPSIS analysis

Dielectric	S_i^*	S_i^-	C_i	TOPSIS Ranking
Si_3N_4	0.237821111	0.487669059	0.672192511	11
Ga_2O_3	0.278908964	0.528118324	0.654399587	12
HfO_2	0.215995485	0.464753144	0.682708895	7
Al_2O_3	0.198620961	0.445669116	0.691721217	6
La_2O_3	0.152382264	0.390361709	0.719237299	1
ZrO_2	0.22528812	0.474645257	0.678129194	9
Ta_2O_5	0.309228018	0.556082744	0.642639348	14
Gd_2O_3	0.188997201	0.434738083	0.696991327	4
$HfSiO_4$	0.220179711	0.469233109	0.680627188	8
$LaAlO_3$	0.233447074	0.48316361	0.674234449	10
$LaLuO_3$	0.154264246	0.392764874	0.717996281	2
MgO	0.190236208	0.436160759	0.69630088	5
TiO_2	0.284920364	0.533779321	0.651984276	13
Y_2O_3	0.188399989	0.434050676	0.697325427	3

Section 2, it can be seen that CBO and κ of the dielectric have a direct impact on the leakage current density. Moreover, it can also be seen that κ has a square-root relationship with the leakage current density whereas CBO has linear relationship. Therefore, the effect of CBO is more on leakage current as compared to the effect of κ. Hence CBO is given the maximum weight of 0.4 which is followed by κ which is given a weight of 0.3. Although E_g of the dielectric has no relationship the leakage current density, it is directly related to the breakdown voltage by the Eq. (1) mentioned in Section 2. So, E_g is given a weight of 0.2. Finally the thermal mismatch $|\Delta\text{TEC}|$ is given the least weight of 0.1. This is because, although $|\Delta\text{TEC}|$ is important in minimizing the interfacial defects, many techniques are available where the defects can be minimized by depositing of the dielectric at nominal temperatures or by using sacrificial layers. So keeping in view the fact that $\sum_{j=1}^{q} w_j = 1$, the weight matrix is $W = [0.4, 0.3, 0.2, 0.1]$.

Using the TOPSIS method one can compute the distance of each material from the ideal solution (S_i^*) and its distance from the non-ideal solution S_i^- and finally the relative closeness of each material to the ideal solution (C_i) can be computed. The ideal solution in the present analysis is given by

$$A^* = (0.216269, 0.19719, 0.0791221, 0.003194)$$

and the non ideal solution is given by

$$A^{-} = (0.018923, 0.03158, 0.027423, 0.051595).$$

The results of these calculations for the current work are shown in the form a table in Table 4. From the table, one can evidently see that La_2O_3 is the closest to the ideal solution which is followed by $LaLuO_3$, Y_2O_3 and Gd_2O_3.

4.3. VIKOR analysis

To perform the VIKOR analysis, the same weighted normalized matrix which was used in TOPSIS analysis is used. Once the decision matrix is obtained, one needs to calculate the group utility G_i and regret R_i of every dielectric material. These values are calculated and are depicted in Table 5.

From the Table 5, one can observe that La_2O_3 has the best Q based ranking which is followed by $LaLuO_3$. Following the approach as described in Section 3.3, one can assign A^1 as La_2O_3 and A^2 as $LaLuO_3$.

$$DQ = 1/N - 1. \tag{17}$$

As there are 14 different dielectrics that are being surveyed in the current analysis, one can use the equation (17) to find the value of DQ to be 0.0769231. Now $Q(A^2) - Q(A^1) = 0.01740$.

From the final step of the VIKOR approach described in Section 3.3, it can be concluded that the best dielectrics are all those which satisfy:

$$Q(A^U) - Q(A^1) \leq DQ. \tag{18}$$

From the Table 6, one can read that $LaLuO_3$ is the only other dielectric that satisfies this criterion. Therefore VIKOR analysis shows that both $LaLuO_3$ and La_2O_3 are equally good choices as gate dielectric for AlGaN−GaN MIS−HEMT.

Hence all the analyses point out that La_2O_3 is the best gate dielectric material for AlGaN/GaN MIS−HEMT device, although TOPSIS analysis also mentions $LaLuO_3$ as another potential alternative. Chao-Wei Lin et al. [38] reported La_2O_3 MIS−HEMT exhibiting best characteristics including the lowest leakage current ($\sim 1\,\mu$A/mm), largest gate voltage swing and pulsed-mode operation. The result of $LaLuO_3$ being another potential dielectric for AlGaN/GaN MIS−HEMT is confirmed by the work of Shu Yang et al. [39], who reported a high I_{ON}/I_{OFF} of 10^9, maximum drain current of 820 mA/mm and steep sub threshold slope of $\sim$ 73 mV/dec. These results show the validity of the proposed analyses.

Table 5. G, R and Q ranks of VIKOR analysis

Dielectric	Gi	G based Rank	Ri	R based Rank	Q	Q based Rank
Si_3N_4	0.670151	3	0.3	4	0.594186	12
Ga_2O_3	0.742516	2	0.32688	3	0.735939	13
HfO_2	0.544379	8	0.226027	12	0.2806	5
Al_2O_3	0.39586	13	0.291781	5	0.287889	4
La_2O_3	0.427761	12	0.205479	13	0.108317	1
ZrO_2	0.609594	6	0.23696	11	0.375568	9
Ta_2O_5	0.822812	1	0.37456	2	0.93726	15
Gd_2O_3	0.525462	9	0.263014	10	0.35209	7
$HfSiO_4$	0.612842	5	0.283562	7	0.493884	11
$LaAlO_3$	0.600398	7	0.26864	8	0.444109	10
$LaLuO_3$	0.463889	11	0.19726	14	0.125721	2
MgO	0.343327	14	0.288493	6	0.225	3
TiO_2	0.624492	4	0.4	1	0.793195	14
Y_2O_3	0.500318	10	0.267123	9	0.336005	6

Table 6. Results of VIKOR analysis

Dielectric	Q value	Q rank	$Q(A^U) - Q(A^1)$	$Q(A^U) - Q(A^1) - DQ$
Si_3N_4	0.594186	12	0.485869	0.408946
Ga_2O_3	0.735939	13	0.627622	0.550698
HfO_2	0.2806	5	0.172283	0.09536
Al_2O_3	0.287889	4	0.179572	0.102649
La_2O_3	0.108317	1	0	−0.07692
ZrO_2	0.375568	9	0.267251	0.190328
Ta_2O_5	0.93726	15	0.828943	0.75202
Gd_2O_3	0.35209	7	0.243773	0.16685
$HfSiO_4$	0.493884	11	0.385567	0.308644
$LaAlO_3$	0.444109	10	0.335791	0.258868
$LaLuO_3$	0.125721	2	0.017403	−0.05952
MgO	0.225	3	0.116683	0.039759
TiO_2	0.793195	14	0.684878	0.607955
Y_2O_3	0.336005	6	0.227688	0.15076

Although, one of the most widely investigated dielectric HfO_2 for silicon based technology is unable to find a considerable rank through material selection methodologies due to its less value of conduction band offset to AlGaN/GaN, but its deposition and process parameters have already been optimized for silicon technology, A_3B_5 compound semiconductors, and for scaled MOS devices [40–43]. This is a great advantage for this dielectric since it becomes cost effective alternative, as one can use the already optimized processes. Whereas, dielectrics like first ranked La_2O_3 whose deposition suffers with the formation of hydroxyl ($La(OH)_3$) [44], needs process optimization. Hence, from a process optimization point of view HfO_2 concedes even the first rank La_2O_3.

5. Conclusion

In this paper, material selection for gate insulator of low leakage AlGaN/GaN MIS−HEMT is done using Ashby's, VIKOR and TOPSIS methods. The conduction band offset values of different dielectrics on AlGaN are analytically computed. These values, along with the band gap, dielectric constant and thermal mismatch magnitude are used to estimate the optimum gate dielectric material. All the approaches show consistency in the results obtained and conclusively point to La_2O_3 as the best dielectric for AlGaN/GaN MIS−HEMT which is closely followed by $LaLuO_3$.

References

[1] M. Riordan. IEEE Spectrum, **41**, 44 (2004).
[2] D. Guo et al. In: *proc. 12th IEEE Intern. Conf. on Solid−State and Integrated Circuit Technology (ICSICT)*, Guilin, China, Oct., 28–31 Oct, 2014.
[3] H.X. Guang, Z.D. Gang, J.D. Sheng. Chin. Phys. B, **24**, 067301 (2015).
[4] W. Lu, L. Wang, S. Gu, D.P.R. Aplin, D.M. Estrada, P.K.L. Yu, P.M. Asbeck. IEEE Trans. Electron. Devices, **58**, 1986 (2011).
[5] J. Chen, T. Kawanago, H. Wakabayashi, K. Tsutsui, H. Iwai, D. Nohata, H. Nohira, K. Kakushima. Microelectron. Reliab., **60**, 16 (2016).
[6] M.V Hove, X. Kang, S. Stoffels, D. Wellekens, N. Ronchi, R. Venegas, K. Geens, S. Decoutere. IEEE Trans Electron Dev., **60**, 3071 (2013).
[7] G. Ye, H. Wang, S. Arulkumaran, G.I. Ng, R. Hofstetter1, Y. Li, M.J. Anand, K.S. Ang, Y.K.T. Maung, S.C. Foo. In: *proc. IEEE 71st Device Research Conf.* (Notre Dame, United States, June 23–26, 2013).
[8] B.Y. Chou et al. IEEE Electron Dev. Lett., **35**, 1091 (2014).
[9] C. Liao et al. IEEE Electron Dev. Lett., **36**, 1284 (2015).
[10] L. Anojkumar, M. Ilangkumaran, V. Sasirekha. Expert Syst. Appl., **41**, 2964 (2014).
[11] K. Kandpal, N. Gupta, J. Mater. Sci. Mater. Electron., **27**, 5972 (2016).

[12] P. Sharma, N. Gupta. J. Mater. Sci. Mater. Electron., **26**, 9607 (2015).
[13] L.M. Wang. In: *proc. 25th Intern. Conf. on Microelectronics* (MIEL 2006) (Belgrade, Serbia and Montenegro, May 14–17, 2006).
[14] H. Zhang, E. J. Miller, E.T. Yu. J. Appl. Phys., **99**, 023703 (2006).
[15] D. Yan, H. Lu, D. Cao, D. Chen, R. Zhang, Y. Zheng. Appl. Phys. Lett., **97**, 153503 (2010).
[16] S. Turuvekere, N. Karumuri, A.A. Rahman, A. Bhattacharya, A. DasGupta, N. DasGupta. IEEE Trans. Electron Dev., **60**, 3157 (2013).
[17] J. Robertson. Eur. Phys. J. Appl. Phys., **28**, 265291 (2004).
[18] R.L. Anderson. Solid State Electron., **5**, 341 (1962).
[19] D.W. Niles, G. Margaritondo. Phys. Rev. B, **34**, 2923 (1988).
[20] J. Robertson. J. Vac. Sci. Technol. B, **18**, 1785 (2000).
[21] J. Robertson, B. Falabretti. J. Appl. Phys., **100**, 014111 (2006).
[22] B.S. Eller, J. Yang, R.J. Nemanich. J. Vac. Sci. Technol. A, **31**, 050807 (2013).
[23] S.P. Grabowski, M. Schneider, H. Nienhaus, W. Monch. R. Dimitrov, O. Ambacher, M. Stutzmann. Appl. Phys. Lett., **78**, 2503 (2001).
[24] S.R. Lee, A.F. Wright, M.H. Crawford, G.A. Petersen, J. Han, R.M. Biefeld. Appl. Phys. Lett., **74**, 3344 (1999).
[25] N. Nepal, J. Li, M.L. Nakarmi, J.Y. Lin, H.X. Jiang. Appl. Phys. Lett., **87**, 242104 (2005).
[26] J. Sanghera, W. Kim, G. Villalobos, B. Shaw, C. Baker, J. Frantz, B. Sadowski, I. Aggarwal. Materials, **5**, 258277 (2012).
[27] S.R. Skaggs. *Zero and low coefficient of thermal expansion polycrystalline oxides* (N LA-6918-MS. Los Alamos Scientific Lab., N. Mex., USA, 1977).
[28] V.B. Braginsky, A.A. Samoilenko. Phys. Lett. A, **315**, 175177 (2003).
[29] R.V. Krishnan, G. Panneerselvam, P. Mankinandan, M.P. Antony, K. Nagarajan. J. Nucl. Radiochem. Sci., **10**, 1926 (2009).
[30] Lorin E. Stevens. *Thermo-Piezo-Electro-Mechanical Simulation of AlGaN (Aluminium Gallium Nitride)/GaN (Gallium Nitride) High Electron Mobility Transistor* (2013) (Master's Thesis, Utah State University, Logan, Utah, 2013).
[31] M.F. Ashby. Acta Mater., **48**, 1792 (2000).
[32] M.F. Ashby. *Material Selection in Mechanical Design*. 2nd edn. (Butterworth–Heinemann, Oxford, 2005).
[33] International Technology Roadmap for Semiconductors (ITRSs). Semiconductor Industry Association, 181 Metro Drive, Suite 450, San Jose, CA 95110 (2006).
[34] A.P. Huang, Z.C. Yang, P.K. Chu. In Hafnium-based high-κ gate dielectrics, ed. by P.K. Chu [Advances in Solid State Circuits Technologies, **446**] (INTECH, Rijeka, 2010).
[35] C. Hwang, K. Yoon. In: *Multiple Attribute Decision Making Methods and Application Survey*, 1st edn (Springer, Berlin, 2005) v. 181, p. 58–191.
[36] S. Opricovic. *Multi-criteria optimization of civil engineering systems* (Faculty of Civil Engineering, Belgrade, 1998).
[37] C.L. Chang. Environ. Monit. Assess., **168**, 339344 (2010).
[38] C.W. Lin, C.W. Yang, C.H. Chen, C.K. Lin, H.C Chiu. In: *proc. Eur. Solid State Device Research Conf.* (Athens, Greece, Sept. 14–18, 2009).
[39] S. Yang et al. IEEE Electron. Dev. Lett., **33**, 979 (2012).
[40] Q. Lu et al. In: *proc. Intern. Semiconductor Device Research Symp.* (Washington, DC, USA, Dec. 5–7, 2001) p. 377–380.
[41] K.P. Huang et al. IEEE Trans. Electron Dev., **63**, 4273 (2016).
[42] L. Trojman. IEEE Lat. Am. Trans., **14**, 4235 (2016).
[43] Y.C. Byun et al. J. Phys. D: Appl. Phys., **45**, 435305 (2012).
[44] L.X. Qian, P.T. Lai, W.M. Tang. Appl. Phys. Lett., **104**, 123505 (2014).